

The evolution of superbubbles and the detection of Ly α in star-forming galaxies

Guillermo Tenorio-Tagle,^{1*} Sergey A. Silich,² Daniel Kunth,³

Elena Terlevich¹ and Roberto Terlevich^{4†}

¹ *Instituto Nacional de Astrofísica Óptica y Electrónica, AP 51, 72000 Puebla, México.*

² *Main Astronomical Observatory National Academy of Sciences of Ukraine, 252650, Kiev, Golosiiv, Ukraine.*

³ *Institut d'Astrophysique de Paris, 98bis Bld Arago, F-75014 Paris, France.*

⁴ *Institute of Astronomy, University of Cambridge, Madingley Road, Cambridge CB3 0HA, UK.*

Accepted ... Received ...; in original form ...

ABSTRACT

The detection of Ly α emission in star-forming galaxies in different shapes and intensities (always smaller than predicted for case B recombination) has puzzled the astronomical community for more than a decade. Here we use two dimensional calculations to follow the evolution of superbubbles and of the H II regions generated by the output of UV photons from massive stars. We show the impact caused by massive star formation in the ISM of different galaxies and we look at the conditions required to detect Ly α emission from a nuclear H II region, and the variety of profiles that may be expected as a function of time.

Key words: H II regions – galaxies: starburst – galaxies: superbubbles – ISM: structure – ISM: evolution – methods: numerical.

1 INTRODUCTION

It has been conjectured that primeval galaxies at large redshift would be easily detected from their Ly α emission (Partridge and Peebles 1967; Meier 1976). Ultraviolet observations of nearby starburst galaxies however, have revealed a much weaker Ly α emission than predicted by simple models of galaxy formation (Meier & Terlevich 1981, Hartmann *et al.* 1984, 1988, Deharveng *et al.* 1986, Terlevich *et al.* 1993, Kunth *et al.* 1997, 1998, 1999). Star-forming galaxies have also been recognized at large redshifts and many of them show weak Ly α emission or none at all (Steidel *et al.* 1996, Lowenthal *et al.* 1997). The reason for the weakness of the Ly α emission has been the subject of a series of debates. It was early realized that pure extinction by dust would be unable to explain the low observed Ly α /H β although this was disputed by Calzetti & Kinney (1992) who tentatively proposed that proper extinction laws would correctly match the predicted recombination value. Valls-Gabaud (1993) on the other hand suggested that ageing starbursts have reduced Ly α equivalent widths affected by strong underlying stellar atmospheric absorptions. Early IUE data has provided evidence for a correlation of Ly α emission and the metallicity of the gas as expected if Ly α is destroyed by dust absorption

(Meier & Terlevich, 1981, Hartmann *et al.* 1988, Terlevich *et al.* 1993). Dust absorption can be particularly effective if multiple scattering in neutral hydrogen selectively increases the path length of these photons through the dusty regions (Auer, 1968). Moreover high density HI regions can also backscatter photons into the H II region in which even a small amount of dust mixed within the ionized gas could be an important agent of destruction. Detailed calculations performed by Chen & Neufeld (1994) show how these effects can lead to Ly α absorptions even for galaxies in which the unattenuated spectrum would show a strong Ly α emission line.

Then, as also shown by Charlot & Fall (1993) the structure of the interstellar medium (porosity and multi-phase structure) is most probably an important factor. As a result the Ly α emission *vs* metallicity correlation should show a large scatter, as evidenced in the recent compilation of 21 local low metallicity starburst galaxy spectra from the IUE archives (Giavalisco *et al.* 1996).

New HST data on ten star-forming galaxies (Lequeux *et al.* 1995; Kunth *et al.* 1997, 1998; Thuan & Izotov 1997) has allowed the further realization that the velocity structure in the interstellar medium plays also a key role in the transfer and escape of Ly α photons (Kunth *et al.* 1997). Three types of observed line profiles have been identified: pure Ly α emission; broad damped Ly α absorption centered at the wavelength corresponding to the redshift of the H II

* e-mail: gtt@inaoep.mx

† Visiting Professor at INAOE.

emitting gas; and Ly α emission with blue shifted absorption features, leading in some cases to P Cygni profiles. As noted by Kunth *et al.* (1998), Ly α emission with deep absorption troughs at the blue side of the Ly α profiles, evidence of a wide velocity field, has been detected in four of the observed galaxies. Interstellar absorption lines (OI, Si II) are also significantly blueshifted with respect to the H II gas.

The velocity and density structure of the neutral gas along the line of sight rather than the abundance of dust particles alone, seem to be the determining factor for the escape of Ly α photons in these objects. Lequeux *et al.* (1995) in the analysis of the HST data of Haro 2, proposed that if most of the neutral gas is outflowing from the ionized region, perhaps in a galactic wind resulting from the intense star formation activity, then Ly α photons will escape (partially) unaffected. If the H I is static with respect to H II, the destroyed Ly α photons are those emitted by the H II region; otherwise, they would correspond to the stellar continuum at wavelengths close to Ly α . Nine out of the ten galaxies show broad Ly α absorption, with a very narrow derived range of logarithmic column densities (19.7 to 21.5 cm⁻²).

Being aware of the complications intrinsic to the transport of Ly α lines, we postulate here a simple scenario that accounts for the variety of Ly α line detections in starburst galaxies. The scenario is supported by two dimensional calculations of multi-supernova remnants evolving in gas-rich disk galaxies covering the range between dwarf and massive galaxies such as the Milky Way (see Sections 2 and 3). The calculations account for the photoionization produced by a massive starburst, and its impact on the surrounding gas as a function of time. Our models are based on the synthetic properties of starbursts, as derived by Mas-Hesse & Kunth (1991) and Leitherer & Heckman (1995); and consider a mechanical energy injection rate ($E_0 \sim 10^{38} - 10^{42}$ erg s⁻¹) which over several 10⁷ yr is equivalent to some tens of thousand of supernova explosions, and the corresponding input of ultraviolet photons generated by the massive stars in the considered cluster. The continuous mechanical energy deposition generates a remnant with an outer shock that sweeps the surrounding gas into a thin shell, while the evacuated cavity is filled with the hot ejecta; efficiently thermalized at the inner shock. The remnant at first decelerates rather rapidly, although its overall expansion allows it to depart from spherical symmetry, given the lower densities away from the galaxy plane. The latter eventually becomes insufficient to cause any further deceleration and the remnant blows out (see Tenorio-Tagle & Bodenheimer 1988; and Silich & Tenorio-Tagle 1998, hereafter referred to as Paper I) allowing for the venting of the hot matter into the galaxy halo. As shown in Paper I, blowout occurs quite early in the evolution, as the superbubbles reach dimensions ~ 1 kpc. This leads to shell fragmentation and to the venting of the processed matter into the extended low density halo where the outer shock forms a new shell of swept up matter. This in the case of dwarf galaxies, initially expands with speeds that well exceed the local escape speed of the galaxy. However, its motion into the gaseous halo causes a continuous deceleration lowering its velocity to values well below the escape speed of the galaxy. These facts are in excellent agreement with detailed observations of dwarf and irregular galaxies which show giant complete remnants expanding at a pace comparable or slower than the escape velocity of

their parent galaxy (see Marlowe *et al.* 1995, Martin 1998). Here we consider the fact that blowout must also allow for the escape of a fraction of the UV radiation produced by the massive members of the starburst, causing an extended H II region into the galaxy halo. The latter is here also held responsible for the escape of UV and Ly α photons from the galaxy. We follow the time evolution of the photoionized region (Section 3) accounting for the drop in stellar luminosity caused by the ageing of the cluster, as well as for the range of recombination times that arises from the different densities that characterize the galaxy haloes and the decelerating shells. The calculations allow us to predict (Section 4) a variety of Ly α profiles that are to be expected from these sources, as a function of time and inclination angle; and a comparison with the existing observations is included in the Discussion section.

2 THE EVOLUTION OF SUPERBUBBLES IN GAS-RICH DISK GALAXIES

2.1 The ISM density distribution

We approximate our galaxies with the prescription for the stellar, dark matter, and gaseous components as given in Paper I and in Li & Ikeuchi (1992). The gas density distribution allows for two isothermal components, related to the central dense molecular core (with a temperature of 100 K^o), and a low density neutral gas halo (with temperature 1000 K^o).

$$\rho_g = \rho_{core} + \langle \rho_{halo} \rangle \quad (1)$$

Both components are supported in a quasi-equilibrium state by rotation and random gas motions with an effective gas pressure

$$P_{ext} = \frac{1}{3}(\rho_{core} C_{core}^2 + \langle \rho_{halo} \rangle C_{halo}^2), \quad (2)$$

where C_{core} is the velocity dispersion of the compact dense core, and C_{halo} that of the extended halo component.

Typical initial density distributions, for several of the cases here considered (see Table 1), are shown in Fig. 1a-c. In all cases the ISM mass amounts to 10 percent of the total mass of the galaxy and ranges from $5 \times 10^7 M_\odot$ in the case of the smallest dwarf galaxies, to $10^{10} M_\odot$ for the more massive disk-like galaxies considered here.

The initial column densities vary between 10^{20} and 10^{23} cm⁻² for different models. Note however, that only a minor part of this value comes from the extended low density halo. Most of the undisturbed gas column density is (as shown in Fig. 2) associated with the central molecular core.

2.2 The starburst mechanical energy and UV radiation input rates

The mechanical luminosity from massive starbursts ($M_{stars} \geq 10^6 M_\odot$) is known to lead to a rapidly evolving superbubble able to blowout from the gaseous galactic disk configuration into the extended H I halo, as E_0 exceeds the energy input rate required for the remnant to reach a typical disk scale-height with a supersonic velocity. As shown by Koo & McKee (1992) if E_0 exceeds the threshold luminosity $L_b = 7.2 \times 10^{36} P_4 H_{100}^2 a_{s,10}$ erg s⁻¹ (where $P_4 =$ disk pressure

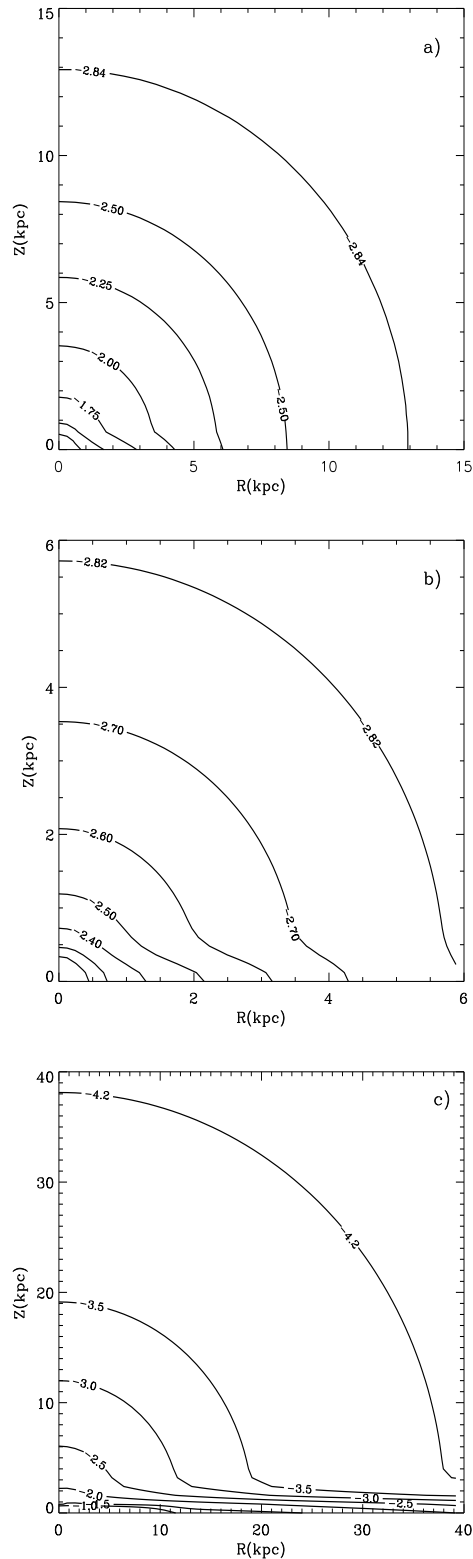


Figure 1. ISM gas distribution. Panels a, b, and c display the initial gas distribution of the 10^9 , 5×10^7 , and $10^{10} M_{\odot}$ for models A, B and C, respectively (see Table 1).

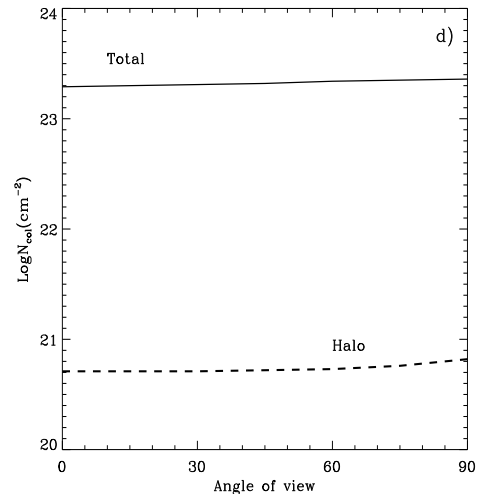


Figure 2. Total and halo initial column density (cm^{-2}) for model A.

in units of $(10^4 k) \text{ cm}^{-3} \text{ K}$, H_{100} is the disk scale height in units of 100 pc and $a_{s,10}$ is the disk sound speed in units of 10 km s^{-1} the superbubble will blowout; thus massive starbursts are expected to lead to the superbubble blowout phenomena even in massive galaxies such as the Milky Way. One can then predict the venting of the hot superbubble interior gas through the Rayleigh-Taylor fragmented shell, into the extended HI halo where it would push once again the outer shock allowing it to build a new shell of swept-up halo matter. A coeval starburst with a total mass larger than several $10^5 - 10^6 M_{\odot}$, also produces an overwhelming ionizing photon flux ($F_{UV} \geq 10^{52} \text{ photons s}^{-1}$) and then blowout must also allow the leakage of at least a fraction of the UV photons emitted by the starburst. These photons are here shown to establish an ionized conical HII region with its apex at the starburst.

It is stellar evolution and the physics of HII regions what defines the time-scales relevant to the evolution, detection and impact that massive bursts of star formation may have on the ISM. Once the mass of a coeval starburst and its IMF are fixed, the integrated mechanical energy power of winds and supernovae will remain almost constant for up to 40 Myr; the life-time of an $8 M_{\odot}$ star. On the other hand, the UV photon production rate will remain constant until the most massive members of the cluster begin to move away from the main sequence (3 – 4 Myr) to shortly end-up as supernovae. From then onwards the starburst flux of UV photons decays rapidly (as t^{-5} ; see Beltrametti *et al.* 1982) and thus after 10 Myr, once the $20 M_{\odot}$ stars have also exploded as supernovae, the HII region gas begins to recombine. Detectability of the ionized gas is thus restricted in the optical and radio recombination lines to 10 Myr, while the impact of winds and supernovae is a much longer lasting event. One can trace in X-rays the thermalized ejected matter either within a superbubble or in a galactic wind emanating from a nuclear starburst, until it cools either adiabatically or by radiation ($t_{cool} = 3kT/(2n\Lambda) \sim 10^8 \text{ yr}$; where n and T are the average density and temperature in the bubble, k is the Boltzmann constant and Λ the corresponding cooling rate). The remnants of the accelerated ISM can also be detected

during a time scale ($\sim 10^8$ yr) that well exceeds the energy deposition time until they slow down to speeds comparable to the random speed of motions of the ISM in their host galaxies (~ 10 km s $^{-1}$). Shells, loops and funnels in a variety of sizes and shapes have been detected in HI and ionized transitions in many starbursts, dwarf, and irregular galaxies (*e.g.* Marlowe *et al.* 1995, Hunter & Gallagher 1997 and Martin 1998)

Our models are restricted to realistic mechanical energy input rates and to the corresponding number of UV photons emitted by the massive members in the stellar clusters. Our standard model A assumes a $10^6 M_{\odot}$ instantaneous starburst with $Z = 0.25 Z_{\odot}$ metallicity, and a Salpeter IMF with a range of stellar masses between 1 and $100 M_{\odot}$, causing a constant mechanical luminosity of 3.5×10^{40} erg s $^{-1}$ for up to 40 Myr. This is consistent with both the synthetic properties of starbursts (see Mas-Hesse & Kunth 1991 and Leitherer & Heckman 1995) and with the values derived by Marlowe *et al.* (1995) from observations of intermediate mass galaxies with a nuclear starburst. The corresponding number of UV photons produced by the massive stars in the cluster ($N_{sb} = 10^{53}$ photons s $^{-1}$) was regulated to remain constant for up to 4 Myr, and then, following stellar evolution models, to drop as $(t/4 \text{ Myr})^{-5}$. A fraction of the UV photons produced by the starburst were assumed to be used within a starburst region, and therefore only $N_{UV} = \varepsilon N_{sb}$ could escape out of the central region and ionizes the superbubble outer shell, and the extended unperturbed halo. Values of ε between 0.1 and 0.7 were used in our grid of models. The mechanical energy input rate and the UV flux produced by the starburst were then linearly scaled with the mass of the host galaxy. This led to values of 1.4×10^{39} erg s $^{-1}$ and 4×10^{51} UV photons s $^{-1}$, for the smallest systems, and 3.5×10^{42} erg s $^{-1}$ and $N_{sb} = 10^{55}$ UV photons s $^{-1}$ for the giant nuclear starbursts in the massive disk galaxies here considered. A second calculation of the massive galaxy powered by a constant star formation rate instead of a coeval starburst is also shown (case C2). In this case the total mechanical energy power and UV radiation flux of case C1 were assumed to remain constant and spread over the 10^8 yr of the considered evolution. The main input parameters that define our galaxies – starburst strength and boundary conditions – are collected in Table 1 which includes in columns 1 – 3 the total mass, the total ISM mass and the central densest ISM mass. Columns 4 and 5 list the radius of the dark matter distribution and the radius of the galaxy’s ISM (see Paper I), C_{halo} and C_{core} are the assumed values for the velocity dispersion of the dense core and the extended halo components; n_0 is the central number density. Columns 9 and 10 list the mechanical power of the assumed starburst and its total UV output. Column 11 lists the assumed metallicity of the ISM and column 12 the starburst life-time. Details of the computational approach used to derive the impact of the ionizing radiation on the evolving giant remnants and the extended halos are given in section 3.

3 THE NUMERICAL MODEL

Our hydrodynamical models describe in detail (see Paper I) the shell morphology, surface density and expansion velocity, as a function of time. The shock velocity,

and post-shock densities and temperatures then follow from the Rankine-Hugoniot jump conditions. The Mach number $M_s = D_s/C_{ism}$ depends on the ionization state of the ISM through the changes in the ambient gas sound velocity

$$C_{ism} = \left(\frac{\gamma k T_{eff}}{\mu} \right)^{1/2}, \quad (3)$$

where the mean mass per particle is $\mu_n = 14/11 m_H$ in the neutral region, and $\mu_i = 14/23 m_H$ within the ionized zone. The effective gas temperature was taken to be

$$T_{eff} = \frac{P_{th}}{kn_g}, \quad (4)$$

where P_{th} is the thermal pressure and k the Boltzmann’s constant. We then calculate the post-shock gas adiabatic - radiative transition with a tabulated cooling function (Gaetz and Salpeter, 1983).

After blowout, and the disruption of the shell via Rayleigh-Taylor instabilities, the hot gas streams out of the cavity with a characteristic velocity of the order of it’s own speed of sound. Therefore we allow the shell to lose mass up to the end of acceleration, when the expansion velocity equals the sound velocity at the bubble center. After blowout the halo gas begins to be collected by a rapid (adiabatic) shock, and a new thin radiative shell forms when the characteristic cooling time exceeds the time interval between blowout and the current evolution time t .

3.1 Shell structure

The structure of the shell of swept-up matter was assumed to be able to develop two concentric zones, and the inner shell surface was derived from the numerically calculated positions. The full thickness of the shell at every Lagrangian mesh is

$$l_s = \frac{\sigma}{n_s \mu_n}, \quad (5)$$

where σ is the shell surface density, and μ_n and n_s are the mean mass per particle and post-shock gas density, respectively. We then calculate the number of photons required to ionize an equivalent spherical shell with the same Lagrangian segment radius R , surface density, and shell number density:

$$N_c = \frac{4\pi}{3} [(R + l_s)^3 - R^3] n_s^2 \alpha_B, \quad (6)$$

where $\alpha_B = 2.59 \times 10^{-13}$ cm 3 s $^{-1}$ is the H recombination coefficient to all levels but the ground state (Osterbrock, 1989). Taking into account the angle α_i between the vector normal to the shell surface and the radius-vector R_i of a particular gridpoint, one can define the ratio

$$\beta = \frac{N_s}{N_c}, \quad (7)$$

where $N_s = N_{UV} \cos \alpha_i$. This allows one to distinguish between three obvious cases along each radial direction: a fully ionized shell ($\beta \geq 1$), a neutral shell ($\beta = 0$), and a partially ionized shell ($0 < \beta < 1$), where all UV photons available are trapped within the shell. In the later case the condition

$$N_s = \frac{4\pi}{3} [(R + l_i)^3 - R^3] n_s^2 \alpha_B, \quad (8)$$

Table 1. Model parameters.

N	M_{tot} $10^{10} M_{\odot}$	M_{gas} $10^9 M_{\odot}$	M_{core} $10^7 M_{\odot}$	R_B kpc	R_G kpc	C_{halo} km/s $^{-1}$	C_{core} km/s $^{-1}$	n_0 cm $^{-3}$	L 10^{40} erg s $^{-1}$	N_{sb} 10^{52} s $^{-1}$	Z/Z $_{\odot}$	t_{burst} Myrs
A1	1.0	1.0	5.0	10	13.6	80	20	1.4×10^3	3.5	10.0	0.3	40
A2	1.0	1.0	5.0	10	13.6	80	20	1.4×10^3	3.5	10.0	1.0	40
A3	1.0	1.0	5.0	10	13.6	80	20	1.4×10^3	3.5	10.0	0.1	40
B1	0.05	0.05	0.1	10	5.9	25	5	18.6	0.14	0.4	0.3	40
C1	10.0	10.0	500.0	20	39.6	150	20	17.0	350	10^3	0.3	40
C2	10.0	10.0	500.0	20	39.6	150	20	17.0	140	4×10^2	0.3	100

where l_i is the thickness of the ionized shell layer should be fulfilled. Combining (8) with equations (6) and (7) gives the ionized skin thickness:

$$l_i = [\beta[(R + l_s)^3 - R^3] + R^3]^{1/3} - R. \quad (9)$$

The width of the neutral skin then follows from the difference between the full shell thickness (5) and the thickness of the ionized layer (9)

$$l_n = R + l_s - [\beta[(R + l_s)^3 - R^3] + R^3]^{1/3}. \quad (10)$$

3.2 The ionization of the ISM

Our simplified approach considers the ionization along a limited number of lines of sight (typically along every 15° from the axis of symmetry) discarding the shell Doppler shift for photon absorption and the UV photons spectral distribution. Photons moving along lines of sight that pinch on neutral sections of the shell, are then used up in its ionization. If the shell segment is in its adiabatic stage, it is then transparent to the ionizing radiation for as long as the post-shock temperature exceeds 10^4 K.

The UV photons that escape the shell cause then the ionization of the halo. Following an ionization equilibrium equation and the on-the-spot approximation, without dust absorption (Osterbrock, 1989), the ionization of each shell section and the corresponding external interstellar gas is considered separately:

$$\Delta(R) = N_{UV} - 4\pi \left(\int_{R_1}^{R_2} n^2(r) \alpha_B r^2 dr + \int_{R_2}^R n^2(r) \alpha_B r^2 dr \right), \quad (11)$$

where R_1 and R_2 are the inner and outer shell radii respectively. The shell densities at every cross-point are linearly interpolated from the values at the nearest Lagrangian points. It was also assumed that within the shell the density varies linearly along lines of sight. Then the first integral (I_1) in equation (11) can be calculated analytically, and reads

$$I_1 = \frac{R_2^3 - R_1^3}{3} \left[n_1^2 + (n_2 - n_1)^2 \frac{R_1^2}{l^2} - 2n_1(n_2 - n_1) \frac{R_1}{l} \right] + \frac{(n_2 - n_1)}{2} \left[n_1 - (n_2 - n_1) \frac{R_1}{l} \right] \frac{(R_2^4 - R_1^4)}{l} + \frac{(n_2 - n_1)^2 (R_2^5 - R_1^5)}{5 l^2}, \quad (12)$$

where $l = R_2 - R_1$ is the shell thickness along a line of sight. The second integral in equation (11) is calculated numerically.

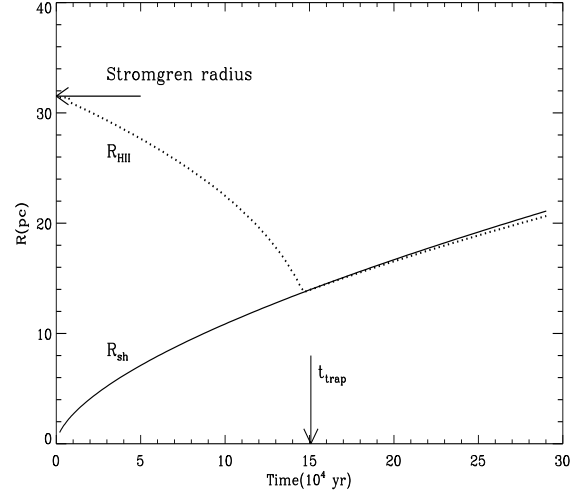


Figure 3. The trapping of the ionization front. The results of a numerical calculation for an ISM gas number density of 10 particle cm $^{-3}$, and an ionizing photon flux of 10^{50} s $^{-1}$. The arrows indicate the analytic predictions for the Strömgren radius and the characteristic time when all UV photons are trapped within the shell of swept-up matter.

The value of Δ is first calculated at the galaxy boundary ($R = R_G$). Positive Δ values represent the escape of UV photons from the galaxy. On the other hand, if Δ is negative, the number of photons is not sufficient to ionize all the halo, and the radius of the H II region is then determined by an iteration procedure to lie between the shock front and the galaxy outer boundary, wherever the value of Δ becomes equal to zero.

After 3.5 – 4 Myr, the number of UV photons produced by the starburst rapidly drops. Also, between 4 – 13 Myr (Models A and B) the leading shock wave moving in the halo becomes radiative and the density within the shell drastically increases (as the square of the Mach number), causing a larger recombination rate. Both processes reduce the UV flux available to keep the galaxy halo fully ionized, and lead to the trapping of the ionization front within the expanding shell.

Our procedure to estimate the trapping of the ionization front, was checked against the analytic formula for a spherical bubble expanding in the preionized homogeneous medium (Comeron 1997), and we found our numerical results in full agreement with analytic predictions (see Fig. 3).

Our procedure also considers the fact that upon photoionization, the recombination time ($\tau_{rec} = 1/n_e \alpha_A \approx$

$10^5/n_{\text{halo}}$ yr) of the low density halo gas may exceed the characteristic dynamical time of the superbubble. This causes the ionized halo to become temporarily transparent to the ionizing radiation. We thus calculate the characteristic recombination time τ_{rec} along different lines of sight and compare this value with a time interval $\tau = t - t_{\text{blowout}}$ between a current time t and the time when a shell section becomes transparent to the starburst UV radiation, causing the ionization of the halo. The number of ionizing photons which escape the galaxy in any direction follows from the equation

$$N_{\text{esc}}(\Theta) = N_{\text{UV}} - N_{\text{trap}}(R_\tau), \quad (13)$$

where Θ is the angle between the direction considered and the symmetry axis. If $\tau_{\text{rec}}(R_G) < \tau$, the halo can only be kept ionized if there is a continuous input of UV photons, and the radius R_τ equals the halo radius ($R_\tau = R_G$). Otherwise, if $\tau_{\text{rec}}(R_G) \geq \tau$, recombination within the densest sections of the galaxy halo will diminish the escape of UV photons. In this case the radius R_τ follows from the condition $\tau_{\text{rec}}(R_\tau) = \tau$.

4 A TYPICAL EVOLUTIONARY SEQUENCE

Fig. 4a shows the evolutionary sequence of our basic model A1. It compares the remnant expansion speed along different angles (Θ) from the symmetry axis with the galaxy escape speed, and indicates the maximum size acquired by the superbubble as a function of time. The shell expansion velocity shows at first a continuous deceleration, followed by a rapid acceleration of the pole sections of the remnant immediately after blowout and shell disruption. During the acceleration phase the shock builds a new shell of swept up halo matter. Afterwards, the remnant speed begins to decline even along the direction perpendicular to the galaxy plane ($\Theta = 0$), as the shock gathers more halo matter. In this way, the remnant ends up expanding with speeds well below the galaxy escape velocity V_{esc} (see also paper I). Nevertheless, after 40 Myrs (the starburst lifetime) a huge remnant has developed and extends in the pole direction almost 5 kpc out of the starburst region (see Fig. 4a). This late phase in the evolution of the remnant, as stated earlier, is unobservable in the optical regime.

Fig. 5(a-f) show the growth of the superbubble as well as the development of the extended ionized zone and its evolution as a function of time. Before 1.5 Myr the dense shell traps all UV photons escaping the central starburst region. However, after blowout and shell disruption, the UV photons escaping the central H II region produce an initially narrow cone of ionized interstellar gas around the symmetry axis. The conical H II region becomes rapidly broader, and at $t \sim 2.5$ Myr it reaches its maximum opening angle. Note that the low density halo matter has a long recombination time ($t_{\text{rec}} = (\alpha n)^{-1} \sim 10^5 \text{yr}/n$; where α is the recombination coefficient and n the local density) and thus upon photoionization it becomes undetectable both in the optical regime and in the 21 cm line and it also becomes transparent to further UV radiation arising from the starburst. After 5 Myr the superbubble leading shock makes a transition from the adiabatic to the radiative regime and matter in the swept up shell begins to recombine. Given the

reduced number of ionizing photons produced by the starburst after 4 Myr and the dilution factor experienced by the UV radiation to reach the recombining shell, rapidly all available photons begin to be used within the shell inhibiting the further leakage of UV radiation into the halo and out of the galaxy. Then, after 8 Myr, the densest parts of the still unshocked halo begin to recombine. Recombination proceeds outwards from the densest unshocked halo regions, forming an increasingly wider layer of neutral gas ahead of the expanding shell (see Fig. 5c).

It is not a straightforward issue to estimate the fraction of Lyman continuum photons that leaks out of galaxies. The only direct observations of the Lyman break in nearby star-forming galaxies are those made by the Hopkins UV telescope (HUT) (Leitherer *et al.* 1995). The analysis suggests that less than 3 percent of the intrinsic Lyman continuum photons escape into the intergalactic medium (Leitherer *et al.* 1995). A more recent analysis of the same data indicates less restrictive values, between 3 percent and 57 percent (Hurwitz *et al.* 1997). Our models predict an early evolutionary phase (between blowout and the trapping of the ionization front within the radiative expanding shell *i.e.* between 3 Myr and 5 Myr for our A1 model) during which a large amount of the UV radiation could leak out of a galaxy into the intergalactic medium (see Fig. 6a). Our predictions seem to be well in line with the observations given that all four star-bursts observed with HUT are much older than 5 Myr (González-Delgado *et al.* 1998) *i.e.* a time when no escape is expected.

The models have assumed that the production of Lyman continuum radiation remains constant for up to 4×10^6 years and then, as the ionizing cluster ages, it drops as t^{-5} causing after 10^7 years (the expected life-time of the central H II region) a depletion in the ionizing radiation of more than two orders of magnitude. An important fraction ($\epsilon = 0.7$) of the initial UV photon production rate was assumed, in all cases shown in Fig. 6, to leak out of the central H II region causing the ionization of the halo and of the recombining sections of the expanding shell. Fig. 6 shows the fraction of UV photons able to escape the galaxy along the conical H II region, as well as the time interval during which this becomes possible. Our results, the same as those from calculations with other values of ϵ , with the exception of the case that assumes a constant star formation rate (Fig. 6d), all show that photoionization of the halo and the escape of UV radiation from the galaxy occurs regardless of the production of UV radiation (and the assumed value of ϵ) and in all cases limited to 5×10^6 years. Given the importance of the escape of the Lyman continuum radiation in relation with estimates of star formation rates, a more detailed analysis of this point is in preparation.

The rapid changes in ionization of the galaxies' ISM have an impact on the neutral gas column density arising from the expanding shell and the halo, and these are central to the transport of the Ly α line emitted by the nuclear H II region which otherwise will be completely absorbed within the extended H I halo. If one for example considers the direction along the axis of symmetry, one would see that immediately after blowout, the ionization of the low density halo, not only favours the direct escape of UV photons out of the galaxy (see Fig. 6a) but also generates a transparent

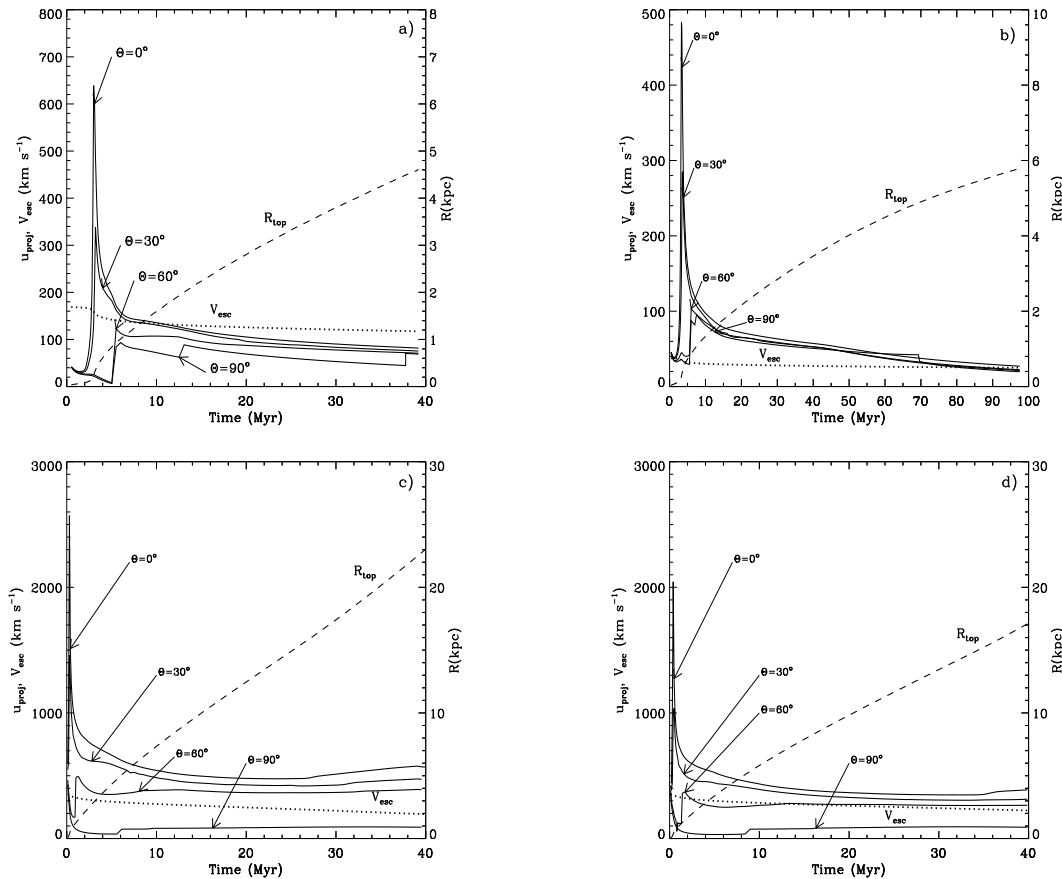


Figure 4. The evolution of superbubbles. Panels a-d display the results for models A1, B, C1 and C2. Solid lines represent the expansion velocities of the superbubbles along different lines of sight (Θ), and as a function of time. These are to be compared with the dotted line which indicates the local escape velocity from a galaxy center at a distance comparable to the maximum dimension of the superbubble (along $\Theta = 0$), indicated by the dashed lines.

region for the Ly α photons produced upon recombination in the central H II region (see Fig. 7).

On the other hand, the leading shock transition from adiabatic to radiative is to deplete the number of UV photons into the halo and out of the galaxy and eventually to cause the trapping of the ionization front within the expanding shell. This situation favours the development of an expanding HI layer and leads to the appropriate conditions (column density and velocity) for the appearance of a blue shifted Ly α absorption feature. In model A1, full ionization of the halo is completed before 3 Myr, and from then onwards and until the expanding shell becomes radiative and traps the ionization front, an observer looking at the central H II region within the ionized halo cone should see the full Ly α line in emission. The trapping of the ionization front occurs at $t \sim 5$ Myrs, when the central starburst is still producing the sufficient number of UV photons to maintain the ionization of the central H II region. This indicates a high probability to observe a blue shifted Ly α absorption feature in intermediate mass galaxies. Recombination in the halo starts after 9 Myr, rapidly enhancing the column density of neutral material and with it the full absorption of the Ly α line produced in the central H II region, irrespective of the line of sight into the galaxy. Panels a, b and c in Fig. 7 show

the run of the HI column density along the axis of symmetry for the standard model A with three different metallicities (models A1-A3). The change in the assumed ISM metal content simply speeds (or delays) the onset of radiative cooling in the expanding shell, and with it the trapping of the ionization front within the shell. Consequently, superbubbles evolving in more metal rich galaxies (as in model A2) will have a shorter lasting phase in which to show Ly α in emission, and a correspondingly longer phase causing a blue-shifted Ly α absorption feature. The converse also holds for more metal poor galaxies (as in model A3).

Despite the similar evolution of the shell expansion velocity, which in all cases shows the same behaviour (at first a continuous deceleration, followed by a rapid acceleration phase after blowout, and a strong deceleration as the bubble ploughs through the extended HI halo) the evolution of superbubbles in other galaxies departs in a variety of ways from our standard case. The fact that remnants of powerful starbursts in massive galaxies, with steep density gradients, retain high expansion speeds (of several hundreds of km s^{-1}) along the polar sectors of their superbubbles for longer periods than their counterparts in less massive galaxies (see Fig. 4) is to be kept in mind. The temperature acquired by the shocked gas being directly related to the shock speed

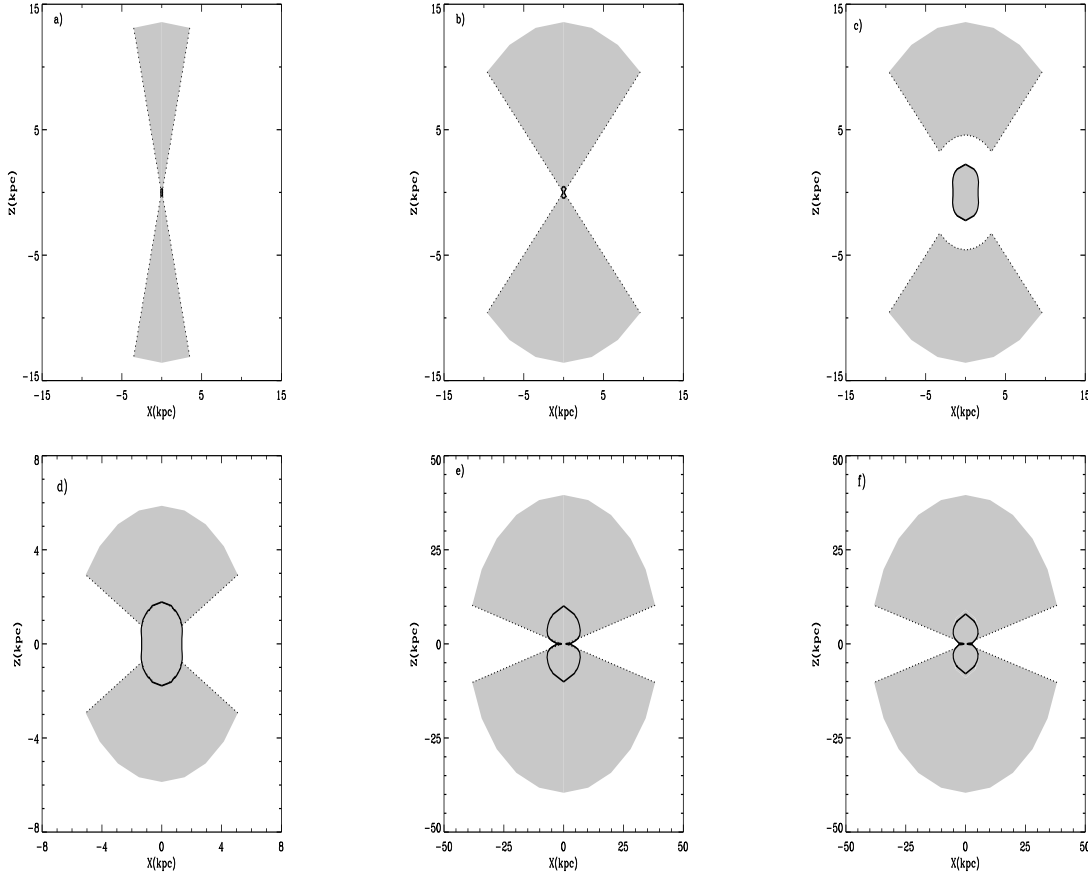


Figure 5. The extended conical H II regions. Cross-sectional views along the symmetry axis display the growth of the superbubble (solid contours) and the development of the conical H II region (shaded area) in model A1 (panels a-c). Note that the H II region extends to the edge of the galaxy, reducing in this way the column density of neutral material within a wide cone. Panels a-c display the evolution after 3.1, 3.5 and 15 Myr. Panel c shows the growth of an increasingly wider shell of neutral matter generated by recombinations in the halo at late evolutionary times. d-f show the results after 15 Myr of evolution for case B, C1, and C2. Note that the low densities in the halos of these galaxies have inhibited recombinations even after the main H II region life-time.

($T_{shock} = 1.4 \times 10^7 (v_{shock}/1000 \text{ km s}^{-1})^2$) implies that these shells are to become radiative at a time that well exceeds both the H II region life-time ($\sim 10 \text{ Myr}$) and the 5×10^7 years span during which the starburst deposits its mechanical energy. Therefore, these galaxies are not likely to produce a blue shifted Ly α absorption feature.

Low mass galaxies appear at first glance as the best candidates to lose their starburst processed metals, or even their ISM (Fig. 1b). However, these systems also experience a rapid shock deceleration as their superbubbles evolve into the galaxy halos, leading as in the standard case A to speeds well below the galaxy escape velocity (see Fig. 4b). Also, as shown in Paper I, if the mass of the galaxy is initially further centrally condensed, then the larger densities and stronger cooling imply an amount of energy much larger than what is observed (see Marlowe *et al.* 1995) for the superbubble to reach the edge of the galaxy. On the other hand, massive disk galaxies with a powerful nuclear starburst generate giant superbubbles able to reach supersonically the outskirts of the galaxy, dumping their processed matter into the intergalactic medium. This happens both in the coeval starburst model (C1) and in the constant star formation rate one (C2) at a time that well surpasses 40 Myr.

Fig. 5d-f show a cross-sectional view of the superbubble and the conical H II region developed after 15 Myr of evolution for cases B1, C1 and C2, respectively. The low density halos in these galaxies inhibit recombination for times that well surpass the H II region life-time. These panels are to be compared with Fig. 5c where the recombination of the halo matter (after 15 Myr of evolution) has led to a broad shell of recombined matter ahead of the evolving superbubble in an intermediate mass galaxy (case A1).

Strong radiative cooling within the expanding shell promotes its transition from adiabatic to radiative and this – if it occurs before $5 \times 10^6 \text{ yr}$ (see Fig. 6) – has an important impact on the number of UV photons leaking into the halo and out of the galaxy. In both, the low and high mass systems here considered, the radiative shell forms much later than in the intermediate mass galaxies, long after the massive stars have moved off the main sequence.

Despite the large value of $\epsilon = 0.7$ used in all calculations presented here, in all models with a coeval starburst the leakage of UV photons into the halo and possibly out of the galaxy is restricted to 5 Myr of evolution by the boundary condition imposed by stellar evolution ($F_{UV} \sim t^{-5}$). The drastic drop in the photon production rate after the most

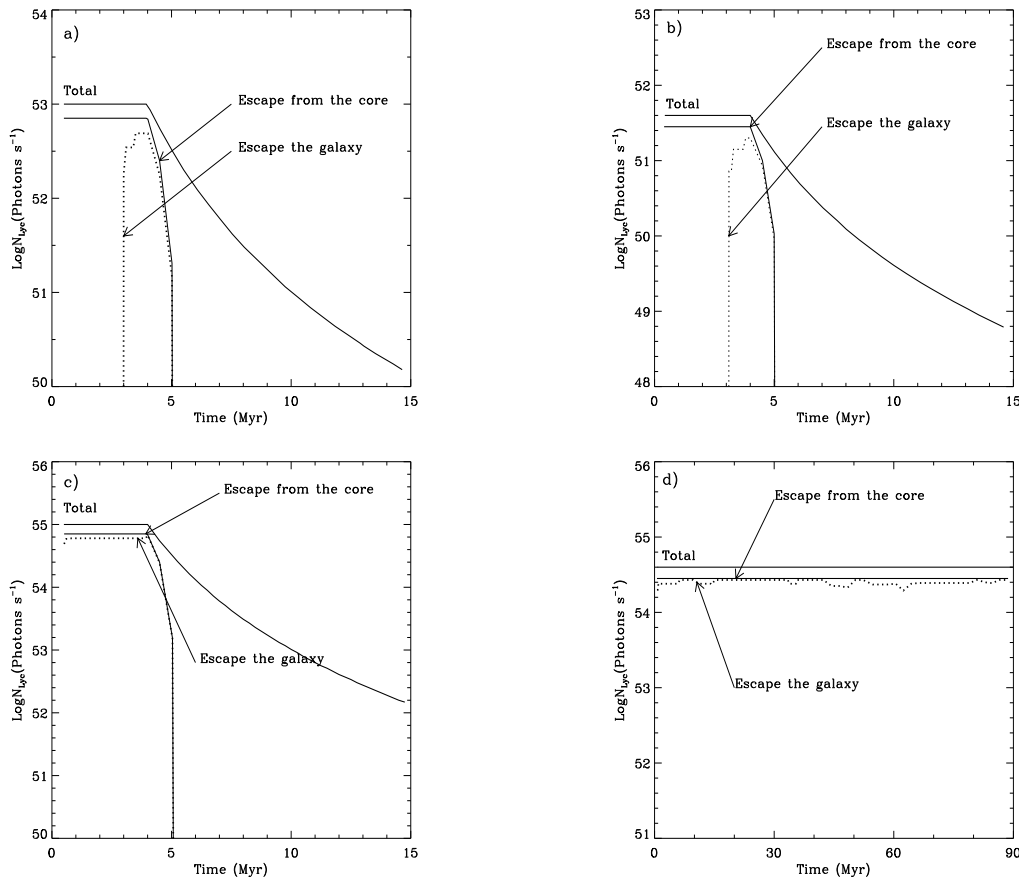


Figure 6. The number of UV photons that escape from a galaxy in models A, B, C1 and C2 are shown in panels a, b, c and d respectively, as a function of time. The escape of UV radiation does not start until the whole galaxy halo is ionized, and in all coeval starburst models (A–C1) it is restricted to 5 Myr by the condition imposed by stellar evolution. Note that given the low densities in the galaxy halos and the corresponding recombination times, these remain ionized for times that well exceed the H II region life-time (10 Myr).

massive stars begin to move off the main sequence, inhibits UV photons to even leak out of the central H II region, and thus clearly calculations with smaller values of ϵ display the same upper limit (see Fig. 6a–c). The situation is different in the constant star formation rate (case C2) where the number of UV photons escaping the galaxy remains almost constant throughout the evolution. This is however also a result of the long recombination time in the low density halo which makes it transparent to the starburst UV flux.

5 DISCUSSION

Our numerical calculations of superbubbles evolving in gas-rich galaxies, accounting for the mechanical energy deposition as well as for the ionization produced by the massive members of a starburst, have led to a more complete picture of the impact that massive star formation may have on a galaxy ISM. We have centered our attention on the time evolution of superbubbles to evaluate the possible burst of processed matter into the intergalactic medium and found that this is only likely for powerful nuclear bursts in disk galaxies. Small and intermediate mass galaxies host superbubbles unable to reach their galaxy outskirts. Furthermore, one should note that the first 10 Myr of evolution, *i.e.* the

H II region life-time, is only a small fraction of the time required for superbubbles to grow and reach their largest dimensions, and thus studies in optical wavelengths can only address the beginning of the evolution and the possible burst into the intergalactic space occurs at much latter times. We have also looked at the extended conical H II region generated by the escape of UV photons from the central starburst once blowout of the superbubble into the extended H I halo takes place. The early blowout into the extended H I halo is promoted by the steep density drop away from the galaxy plane, causing the burst of the thermalized ejected matter as well as the leak of UV radiation into the extended halo (see Fig. 8a, b). The evolution of the H II region is central to the transport and detection of Ly α emission from the central H II region. For example, once recombination starts in the fast expanding shell, it will cause a correspondingly blueshifted Ly α emission, as depicted in Fig. 8c. Once the shell presents a large column density ($\sim 10^{19} \text{ cm}^{-2}$), as it grows to dimensions of a few kpc, it will trap the ionization front. This is promoted by the large shell densities and the geometrical dilution of the ionizing radiation. Note that from then onwards, recombinations in the shell will inhibit the further escape of ionizing photons from the galaxy (compare Fig. 8b, c, and d). The trapping of the ionization front,

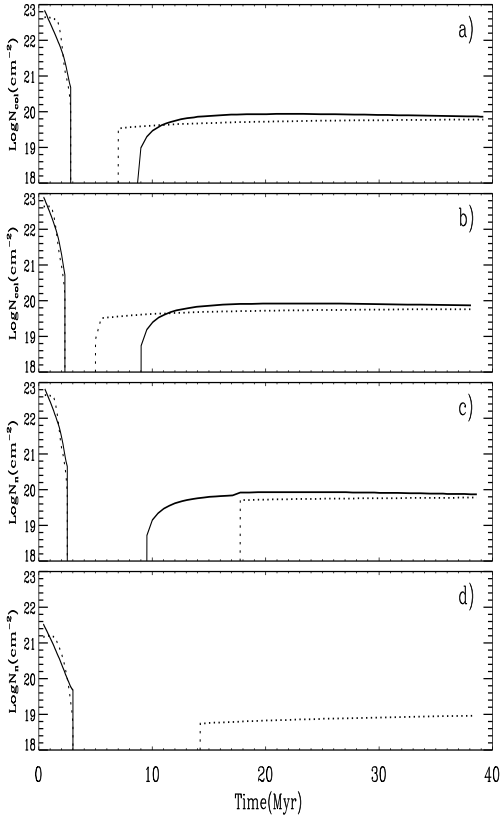


Figure 7. The neutral gas column density variation along the symmetry axis for models A1, A2, A3, and B are shown respectively in panels a – d. Solid lines indicate the unshocked component and the dotted lines the column density arising from the recombinating shell.

makes the shell acquire a multiple structure with a photoionized inner edge, a steadily growing central zone of H I, and an outer collisionally ionized sector where the recently shocked ionized halo gas is steadily incorporated. The growth of the central layer eventually will cause the sufficient scattering and absorption of the Ly α photons emitted by the central H II region, leading to a blueshifted Ly α absorption. Note also that for as long as recombinations continue to occur at the leading edge of the shell, a blueshifted Ly α in emission will appear superposed on the blueshifted absorption feature (see Fig. 8d). Recombination at the leading edge of the shell will become steadily less frequent, depleting the blueshifted Ly α in emission. This is due when the shell and its leading shock move into the outer less dense regions of the halo, and the shell recombination time, despite the compression at the shock, becomes larger than the dynamical time. At this stage, an observer looking along the conical H II region will detect a P-Cygni-like Ly α line profile as shown in Fig. 8e.

The geometrical dilution of the UV flux will begin to make an impact as the superbubble grows large. This, and the drop in the UV photon production rate caused by the death of the most massive stars after $t = t_{ms}$, will enhance the column density of neutral material in the central zone of the recombined shell to eventually cause the full saturated absorption of the Ly α line (see Fig. 8f). Full saturated absorption has usually been accounted for by the large column

density of the extended H I envelope of these galaxies and thus, as in all models, many different orientations will suit the observations. In our scenario however, also when observing within the solid angle defined by the conical H II region formed after blowout, such broad absorptions could arise well after blowout, once a large column density of shocked neutral material ($N \geq 10^{20} \text{ cm}^{-2}$) has formed ahead of the trapped ionization front.

The solid angle subtended by the ionized cone will be a rapidly changing function of time, particularly during the early stages of evolution, immediately after blowout. However, numerical experiments and observations (see Paper I, and Tenorio-Tagle & Muñoz-Tuñón 1997, 1998 and references therein) restrict this to a maximum value of about 70° , with the walls of the superbubble near the galaxy plane inhibiting its further growth.

P-Cygni Ly α profiles are predicted when observing along the angle subtended by the conical H II region but only once the ionization front is trapped by the sector of the superbubble shell evolving into the extended halo. This will produce the fast moving layer of H I at the superbubble shell, here thought to be responsible for the partial absorption observed in sources such as Haro 2, ESO 400-G043 (which probably exhibits a secondary blueshifted Ly α emission) and ESO 350-IG038 (Kunth *et al.* 1998). In the latter case however, the profile is not typical of a clear P-Cygni profile. Instead the underlying damped Ly α absorption extends beyond the red of the line emission. Damped Ly α absorption is shown by several galaxies. We note that these objects are all gas rich dwarf galaxies whereas in most cases but Haro 2, the galaxies that exhibit Ly α in emission or with a P-Cygni profile, are on the higher luminosity side of the distribution ($M \leq -18$). Pure Ly α emission is observed in C0840+1201 and T1247-232 (Terlevich *et al.* 1993; IUE) or T1214-277 (Thuan & Izotov 1997; HST). Such a line implies no absorption and thus no H I gas between the starburst H II region and the observer, as when observing the central H II region after the superbubble blowout, within the conical H II region sector carved in the extended H I halo.

The main implication of our calculations is that it is the feedback from the massive stars what – through ionization and the evolution of superbubbles – leads to the large variety of Ly α emission profiles. The escape of Ly α photons depends sensitively on the column density of the neutral gas and dust following the suggestion that the attenuation by dust is enhanced by scattering with hydrogen atoms. Note that apart from the observed profiles: Ly α in emission, P-Cygni-like profiles and full saturated absorption (as in Fig. 8 a, b, e and f) the scenario predicts also secondary blueshifted Ly α emission profiles emanating from the rapidly expanding and recombinating shell (see Fig. 8c and d). If massive star formation leads also to networks of shells such as those observed in 30 Dor (Chu & Kennicutt 1992) one should also expect a forest of Ly α in emission arising from recombinations in the various expanding shells in the network.

ACKNOWLEDGMENTS

The authors wish to thank the Guillermo Haro Advanced program of Astrophysics at INAOE, during which this work was completed. GTT, ET and RT acknowledge support from

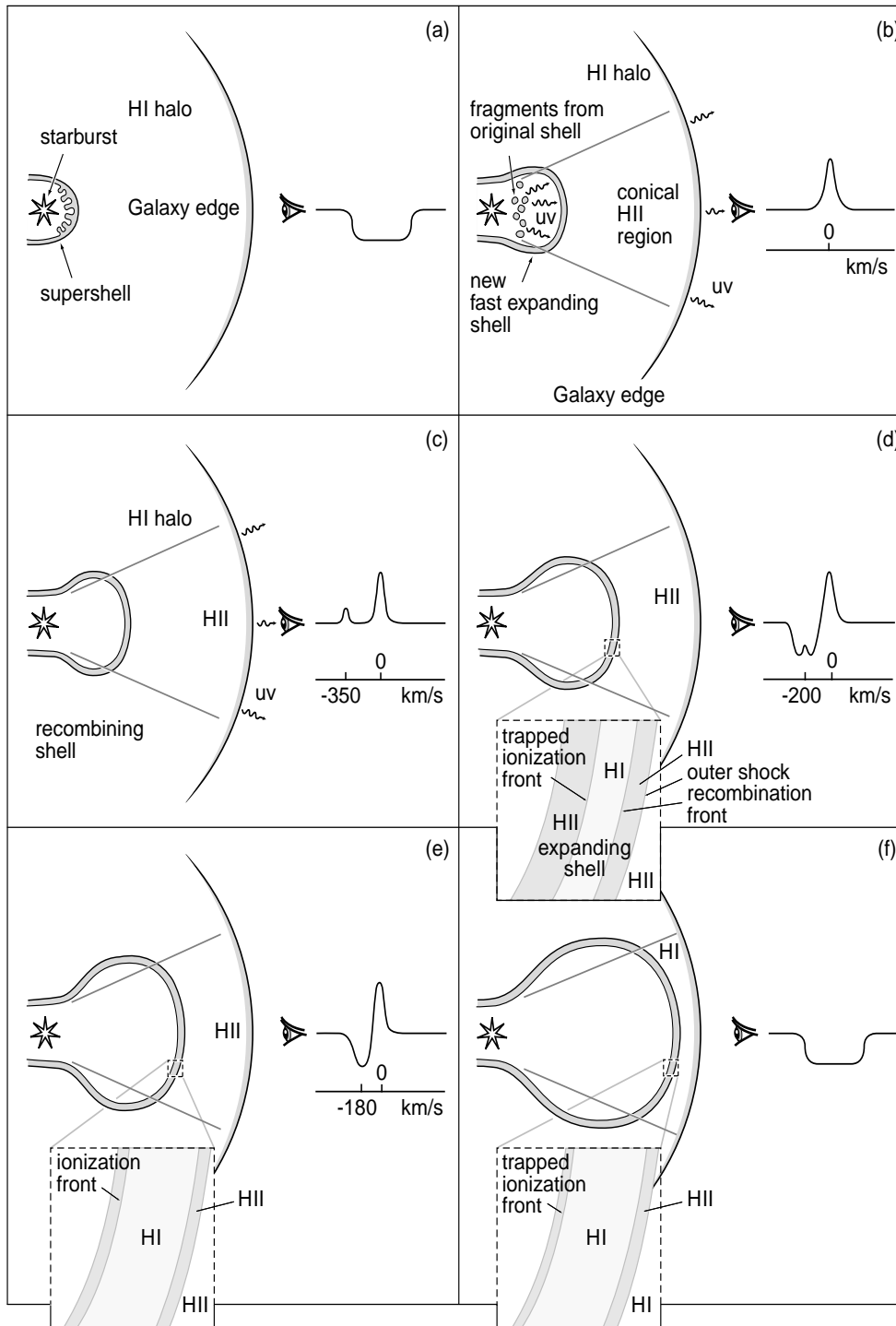


Figure 8. The evolution of superbubbles and the $\text{Ly}\alpha$ emission profile expected from star-forming galaxies. The panels present the sequence of changes in the structure of the ISM produced by the evolution of a massive starburst. On the right hand-side of each panel, the $\text{Ly}\alpha$ profile expected is shown and the scale corresponds to model A1 at times (a) $\leq 1.5\text{Myr}$, (b) $\sim 2.5\text{Myr}$, (c) $\sim 4\text{Myr}$, (d) $\sim 5\text{Myr}$, (e) $\sim 6\text{Myr}$ and (f) $> 8\text{Myr}$. The sequence starts with a giant superbubble which is about to burst into the extended HI halo of a galaxy, as its shell of swept up matter becomes Rayleigh - Taylor unstable (a). The instability leads to the rupture of the shell and with it to the exit of the thermalized stellar ejecta which then freely streams and promotes the development of a new shock and a new shell of swept up halo material (b). At the same time, the stellar uv radiation is able to leak out into the halo, and even beyond the galaxy outer edge, leaving behind an extended, low density, conical HII region. Recombinations in the shell of swept up halo matter should become increasingly more important as a function of time, causing a blueshifted $\text{Ly}\alpha$ emission and a depletion in the number of ionizing photons escaping the galaxy. The latter will be totally depleted once the ionization front is trapped by the recombining shell (c and d). The last stages in the evolution enhance the column density of HI in the recombining shell leading to a P-Cygni $\text{Ly}\alpha$ profile and eventually to a full saturated absorption (e and f).

an EC – EARA – grant and CNRS during visits to IAP where part of this work was accomplished. SAS acknowledges support from the Royal Society grant for joint projects with the former Soviet Union, and the RGO and the IoA in Cambridge for partial financial support. SAS also thanks the INAOE – while ET thanks the RGO and IoA – for hospitality and partial financial support. We thank Stephan Charlot and Max Pettini for comments and suggestions and Richard Sword from the IoA for his help with the drawing of Fig. 8.

REFERENCES

- Auer L. 1968, *A&A*, 153, 783
 Beltrametti M., Tenorio-Tagle G. & Yorke, H. W. 1982, *A&A*, 112, 1
 Calzetti D. & Kinney A.L. 1992, *ApJ*, 399, L39
 Charlot S. & Fall S.M. 1993, *ApJ*, 415, 580
 Chen W.L. & Neufeld N.A. 1994, *ApJ*, 432, 567
 Chu Y H. & Kennicutt R. 1992, *ApJ*, 425, 720
 Comeron F. 1997, *A&A*, 326, 1195
 Deharveng J.M., Joubert M. , Kunth D. 1986, in the First IAP workshop: “Star-Forming Dwarf Galaxies and related objects”, edited by. D. Kunth, T.X. Thuan and J. Tran Thanh Van, Editions Frontieres, p.431
 Gaetz, T. J. & Salpeter, E.E. 1983, *ApJS* 52, 155
 Giavalisco M., Koratkar A. & Calzetti D. 1996, *ApJ*, 466, 831
 González Delgado, R.M, Leitherer, C., Heckman, T., Lowenthal, J.D., Ferguson, H.C. & Robert, C. 1998, *ApJ*, 495,698
 Hartmann L.W., Huchra J.P. , Geller M.J. 1984, *ApJ*, 287, 487
 Hartmann L.W., Huchra J.P., Geller M.J., O’Brien P. & Wilson R. 1988, *ApJ*, 326, 101
 Hunter, D. A. & Gallagher, J. S. 1997, *ApJ*, 475, 65
 Hurwitz, M, Jelinsky, P., Dixon, W. van Dyke, 1997, *ApJ* 481L, 31
 Koo, B-C. & McKee, C. F.: 1992, *ApJ*, 388, 93
 Kunth D., Lequeux J., Mas-Hesse J.M., Terlevich E. & Terlevich R. 1997, *Rev. Mex. Astr. Astrofis.* 6, 61
 Kunth D., Mas-Hesse J.M., Terlevich E., Terlevich R., Lequeux J. & Fall M. 1998, *A&A*, 334, 11
 Kunth D., Terlevich E., Terlevich, R. & Tenorio-Tagle , G. 1999, astro-ph/9809096, proceedings of “Dwarf Galaxies and Cosmology” ed. T.X.Thuan et al. (Editions Frontieres, Gif-sur-Yvette)
 Leitherer C. & Heckman T.M. 1995, *ApJS*, 96,9
 Leitherer C., Ferguson H.C., Heckman T.M. & Lowenthal J.D. 1995, *ApJ*, 454, L2
 Lequeux J., Kunth D., Mas-Hesse J.M. & Sargent W.L.W. 1995, *A&A*, 301, 18
 Li, F. & Ikeuchi, S. 1992, *ApJ*, 390, 405
 Lowenthal J.D., Koo, D.C., Guzmán, R., Gallego, J., Phillips, A.C., Faber, S.M., Vogt, N.P., Illingworth, G.D. & Gronwall, C. 1997, *ApJ*, 481, 673
 Marlowe, A.T., Heckman, T.M., Wyse, R.F.G. & Schommer, R. 1995, *ApJ*, 438, 563
 Martin, C. L. 1998, *ApJ*, 506, 222
 Mas-Hesse, J.M. & Kunth, D., 1991, *A&AS*, 88, 399
 Meier D.L. 1976, *ApJ*, 207, 343
 Meier D.L. & Terlevich R. 1981, *ApJ*, 246, L10
 Osterbrock D.E. 1989, *Astrophysics of Gaseous Nebulae and Active Galactic Nuclei*. Univ. Sci. book, 408p.
 Partridge R. & Peebles P.J.E. 1967, *ApJ*, 146, 868
 Silich S. & Tenorio-Tagle G. 1998, *MNRAS* 299, 249
 Steidel C.C., Giavalisco M., Pettini M., Dickinson M. & Adelberger K. 1996, *ApJ*, 462, 17
 Tenorio-Tagle G., Marlowe, A.J. & Bodenheimer, P. 1988, *ARA&A* 26, 145
 Tenorio-Tagle G. & Muñoz-Tuñón 1997, *ApJ*, 478, 134
 Tenorio-Tagle G. & Muñoz-Tuñón 1998, *MNRAS* 293, 299
 Terlevich E., Diaz A.I., Terlevich R. & Garcia-Vargas M.L. 1993, *MNRAS* 260, 3
 Thuan T.X. & Izotov Y.I. 1997, *ApJ* 489, 623
 Valls-Gabaud D. 1993, *ApJ*, 419,7